

Unlearnable Examples Give a False Sense of Data Privacy: Understanding and Relearning

Pucheng Dang, Xing Hu* *Member, IEEE*, Kaidi Xu *Member, IEEE*, Jinhao Duan,
Di Huang, Husheng Han, Rui Zhang, Zidong Du *Member, IEEE*,

Abstract—Unlearnable examples are proposed to prevent third parties from exploiting unauthorized data, which generates unlearnable examples by adding imperceptible perturbations to public publishing data. These unlearnable examples proficiently misdirect the model training process, leading it to focus on learning perturbation features while neglecting the semantic features of the image. In this paper, we make an in-depth analysis and observe that models can learn both image features and perturbation features of unlearnable examples at an early training stage, but are rapidly trapped in perturbation features learning since the shallow layers tend to learn on perturbation features and propagate harmful activations to deeper layers. Based on the observations, we propose *Progressive Staged Training*, a self-adaptive training framework specially designed to break unlearnable examples. The proposed framework effectively prevents models from becoming trapped in learning perturbation features. We evaluated our method on multiple model architectures over diverse datasets, e.g., CIFAR-10, CIFAR-100, and ImageNet-mini. Our method circumvents the unlearnability of all state-of-the-art methods in the literature, revealing that existing unlearnable examples give a false sense of privacy protection and provide a reliable baseline for further evaluation of unlearnable techniques.

Index Terms—Robust machine learning, privacy security, unlearnable example countermeasures.

I. INTRODUCTION

DEEP neural networks (DNNs) have significantly boosted computer vision techniques in the past decade and achieved even better capabilities surpassing human beings [1]–[15]. One of the most important factors contributing to the great success comes from the representative and valuable data collected for training. Not only influential public datasets such as CIFAR [16] and ImageNet [17] are proposed for benchmark evaluation, but also huge volumes of scenario-sensitive data are used for real model training and deployment [18]–[21]. Data has become an important asset and ensuring authorized access to sensitive data is crucial.

Pucheng Dang and Husheng Han are with the SKL of Processors, Institute of Computing Technology, CAS, Beijing 100190, China, the University of Chinese Academy of Sciences, Beijing, 100049, China. E-mail: {dangpucheng20g.hanhusheng20z}@ict.ac.cn

Xing Hu and Zidong Du are with the SKL of Processors, Institute of Computing Technology, CAS, Beijing, 100190, China, Shanghai Innovation Center for Processor Technologies, Shanghai, 201210, China. E-mail: {huxing.duzidong}@ict.ac.cn

Kaidi Xu and Jinhao Duan are with the Department of Computer Science, College of Computing & Informatics, Drexel University, Philadelphia, 19104, USA. E-mail: {kx46.jd3734}@drexel.edu

Huang Di and Rui Zhang are with the SKL of Processors, Institute of Computing Technology, CAS, Beijing, 100190, China. E-mail: {huangdi.zhangrui}@ict.ac.cn

*Corresponding authors: Xing Hu

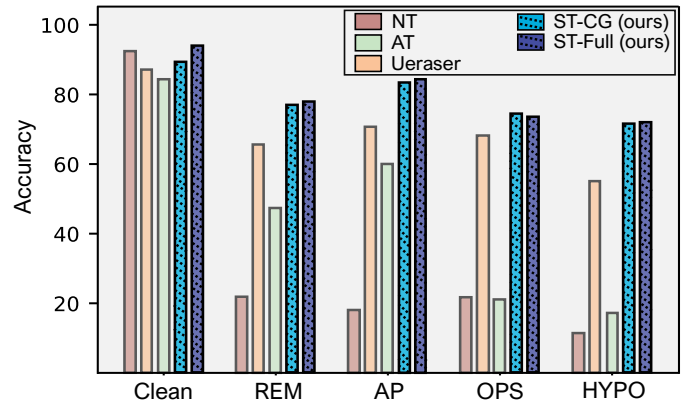


Fig. 1. Test accuracy of a ResNet-18 with normal (NT), adversarial (AT), Chroma-CVE and ST series trained (ours) on various unlearnable protected CIFAR-10 datasets such as REM [22], SP [23] OPS [24] and HYPO [25]. The results reflect that our training method ST defeats the data protection capability of these unlearnable methods and is highly effective in preserving clean accuracy.

A. Current Research Status of Unlearnable Example

Previous studies propose “unlearnable example” techniques to address unauthorized access to sensitive data [22]–[24], [26]–[28]. Specially, Yu *et al.* [23] found that perturbations act as shortcuts [29]–[34] to mislead models to a bad state. These unlearnable examples are generated by injecting carefully crafted, imperceptible perturbations into the training data, which causes models to focus on learning irrelevant perturbation features rather than the meaningful semantic features of natural images. Meanwhile, some data poisoning attacks [25], [35]–[38] aim to manipulate the performance of a machine learning model via injecting maliciously poisoned examples into its training set, and such attacks can also be employed for data protection purposes.

To address the challenge of learning from unlearnable samples, several approaches have been proposed [39]–[42]. Ueraser [39] employs data augmentation techniques to reduce the impact of unlearnable perturbations. LE [40] and AVATAR [41] utilize popular diffusion models to filter out these unlearnable perturbations. However, these approaches primarily focus on data processing methods for handling unlearnable samples, rather than investigating how unlearnable perturbations function from a model learning perspective or exploring ways to mitigate the influence of such perturbations through improvements in the model’s learning process.

B. Motivations and Observations

To address this research gap, we investigate the vulnerabilities of unlearnable examples from a model learning perspective

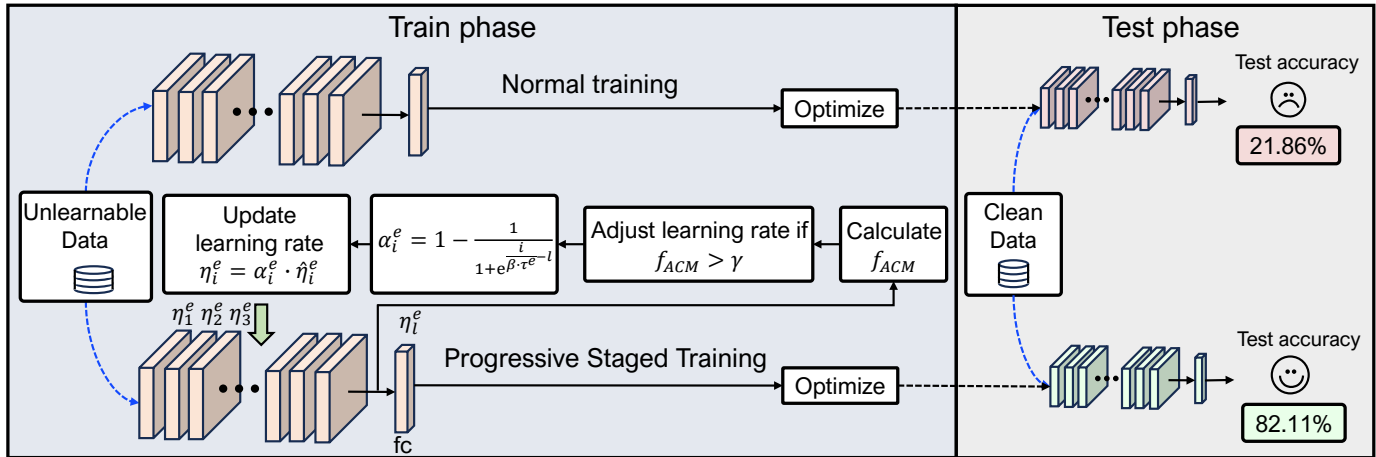


Fig. 2. An overview of ST when countering unlearning perturbations. Compared with normal training, once the indicator ACM (Eq. (4)) detects unlearnable perturbation feature learning, progressive staged training (ST) recovers clean accuracy of unlearnable examples by adjusting the learning rate of each layer (Eq. (5)).

and design methods to neutralize them by adjusting the model’s learning process. We initially examine the differential behaviors exhibited by the model when presented with unlearnable examples versus clean examples. Specifically, we make the following observations: 1) In the early stages of training, models learn both unlearnable perturbation features and image semantic features. However, in subsequent stages, the focus shifts exclusively to the acquisition of unlearnable perturbation features. This observation reveals that unlearnable examples are indeed capable of being learned: by guiding the model to focus on image semantic features after the initial training phase, it is possible to extract semantic knowledge from samples initially deemed unlearnable. 2) Compared to deeper layers, correctly guiding the model’s shallow layers to learn image semantic features plays a crucial role in preventing the model from becoming trapped in learning unlearnable perturbation features. When shallow layers are trapped in learning unlearnable perturbation features, detrimental activation is propagated through these layers, contaminating deeper layers and increasing their propensity for wrong learning. This observation indicates that the quality of shallow-layer training is significantly correlated with the overall tendency of the model to break through unlearnable perturbation learning.

C. Contributions

Based on these observations, we provide the following suggestions: 1) Models can extract valid semantic features from unlearnable examples during the initial phase of training. 2) Correctly guiding the model’s shallow layers to learn image semantic features is the key to defeating unlearnable examples. In this case, we propose a training paradigm called Progressive Staged Training (ST). ST aims to prevent models from becoming trapped in unlearnable perturbation feature learning. ST assesses whether the models are in the wrong learning process and implements a progressive, staged strategy for training that involves dynamically adjusting the learning rate. To quantitatively evaluate whether the model is trapped in the wrong learning process, we propose Activation Cluster Measurement (ACM), based on the insight that unlearnable

perturbation features have a larger inter-class distance and smaller intra-class distance [23] in a low dimension space. To demonstrate the efficacy of ST, we conduct comprehensive experiments with multiple model architectures on CIFAR-10 [16], CIFAR-100 [16], and ImageNet-mini. Experimental results show that ST significantly defeats existing unlearnable techniques, thereby providing a dependable benchmark for the subsequent evaluation of samples considered unlearnable.

The scope of this paper is to invalidate unlearnable examples, and our method is a special design for unlearnable examples. As shown in Fig. 1, our method prevents models from the trap caused by unlearnable perturbation. Furthermore, it has proven to be highly efficient in maintaining accuracy with clean data. We summarize our contributions as follows:

- We demonstrate how models can learn valid image semantic features from initially unlearnable examples during the early stages of training. Guiding shallow layers to learn image semantic features substantially aids in defeating unlearnable examples.
- We propose a learning framework, ST, to prevent models from being trapped in unlearnable perturbation feature learning, with the help of ACM metric for quantitatively evaluating whether the model is in the wrong learning process.
- We perform comprehensive experiments to show that our ST framework breaks all state-of-the-art unlearning samples in the literature on multiple model architectures across various datasets.

II. RELATED WORK

Unlearnable examples [22]–[24], [26]–[28] share similar mechanisms as data poisoning attacks [25], [35]–[38] but serve different application scenarios. The unlearnable example is a data protection method that adds imperceptible perturbations to the entire dataset. Suppose we have a dataset consisting of original clean examples $\mathcal{D}_{clean} = \{(\mathbf{x}_i, y_i)\}_{i=1}^n$ drawn from a distribution \mathcal{S} , where $\mathbf{x}_i \in \mathcal{X}$ is an input image and $y_i \in \mathcal{Y}$ is the associated label. We assume that the unauthorized parties will use the published training dataset to train a classifier

$f_{\theta} : \mathcal{X} \rightarrow \mathcal{Y}$ with parameter θ . Error-minimizing (EM) [26] perturbations are produced by an alternating bi-level min-min optimization on both model parameters and perturbations:

$$\arg \min_{\theta} \mathbb{E}_{(x_i, y_i)} \left[\min_{\delta_i} \mathcal{L}(f_{\theta}(x_i + \delta_i), y_i) \right] \quad (1)$$

where \mathcal{L} is the cross entropy loss and $\|\delta_i\|_{\infty} < \epsilon$. Being induced to trust that the perturbation can minimize the loss better than the original image features, the model will pay more attention to the perturbations. However, EM perturbations have no defense on adversarial training which adds random perturbations to input while training to improve the robustness of models. To solve this problem robust error-minimizing (REM) [22] perturbations implement adversarial training while generating unlearnable perturbations, which grants perturbations the ability to resist adversarial training. Yu, *et al.* found that perturbations act as shortcuts to mislead models to a bad state, and proposed synthetic perturbations (SP) [23] which generate unlearnable perturbations without the optimization of error-minimization. One-pixel shortcut (OPS) [24] used a perceptible pixel as the perturbation to protect data. To improve the transferability of unlearnable perturbations, Ren, *et al.* proposed transferable unlearnable examples [27], which protects data privacy from unsupervised learning. However, such unlearnable examples are a special design for unsupervised learning and do not perform well with adversarial training. Unlearnable Clusters [28] provides unlearnable examples for label-agnostic learning in which attackers could define labels by themselves.

Meanwhile, some data poisoning attacks [25], [35], [36] aim to manipulate the performance of a machine learning model via injecting maliciously poisoned examples into its training set and such attacks can also be employed for data protection purposes. Adversarial Examples as Poisons (AEP) [35] show that adversarial examples with the original labels are strong poisons at training time. Hypocritical perturbations (HYPO) [25] considers the adversarial sample generation and uses a pre-trained surrogate to generate adversarial samples for unlearnability. Autoregressive poisoning (AP) [36] proposes a generic perturbation that can be applied to different datasets and architectures.

Recent works have explored learning from unlearnable samples. Ueraser [39] employs data augmentation techniques to mitigate the impact of unlearnable perturbations. LE [40] and AVATAR [41] utilize popular diffusion models to filter out these unlearnable perturbations. These approaches primarily focus on data processing methods for handling unlearnable samples, whereas our work is orthogonal, aiming to optimize the learning process by dynamically adjusting the learning rate to effectively learn from such samples.

III. METHOD

In this section, we first present our observations and insights into the training process involving unlearnable examples. Our findings reveal two key insights into the learning process of models trained on unlearnable examples. Building upon these insights, we introduce Progressive Staged Training (ST), a novel training framework that learns image semantic features

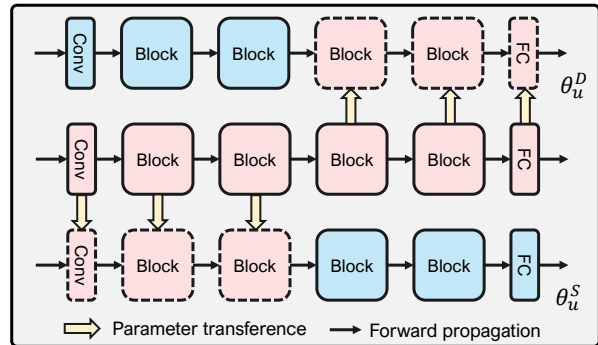


Fig. 3. The sketch of θ_u^D and θ_u^S . Their weights come from a model trained on clean data (middle row) by replacing deep or shallow layers. The result of θ_u^S and θ_u^D trained on unlearnable data can be found in Fig. 4.

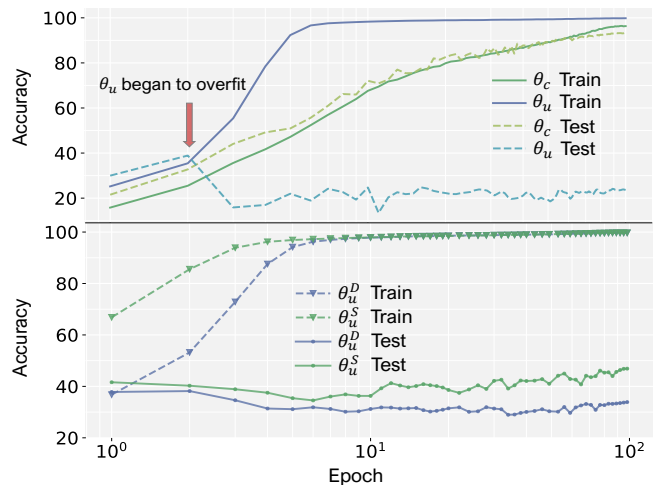


Fig. 4. **Top**: the training and test accuracy of a ResNet-18 trained on clean data (θ_c) and unlearnable data (θ_u). As indicated by the orange arrow, after epoch 3 the training accuracy of θ_u increases sharply, while the test accuracy of θ_u significantly decreases, implying θ_u is trapped in the unlearnable perturbation features. **Bottom**: the training and test accuracy of θ_u^S (green) and θ_u^D (blue) on unlearnable data. θ_u^S performs better accuracy proving that shallow layers are more crucial for a model to learn correct features during training.

from unlearnable examples. We further propose Activation Cluster Measurement (ACM), a novel determinant employed to ascertain whether the comprehensive model is succumbing to learning unlearnable perturbation features.

A. Observations and Insights

*Insight 1: Model learns both image semantic feature and unlearnable perturbation features at the **early** stage before being trapped in unlearnable perturbation feature learning, which provides a “golden window” for image semantic feature learning.* To demonstrate this insight, we show the learning process of a ResNet-18 on unlearnable CIFAR-10 in Fig. 4 (more results of other architectures and datasets can be found in Sec. IV-C1). The generation of unlearnable perturbations is designed to make it easier for the model to achieve its learning objective (a lower loss function value). As a result, the model develops a preference for these perturbation features, which act as “lures”, causing it to neglect the learning of semantic features from the images. This mechanism serves as a means of data protection. As shown in Fig. 4, the training accuracy of the model continues to increase, while the testing accuracy remains

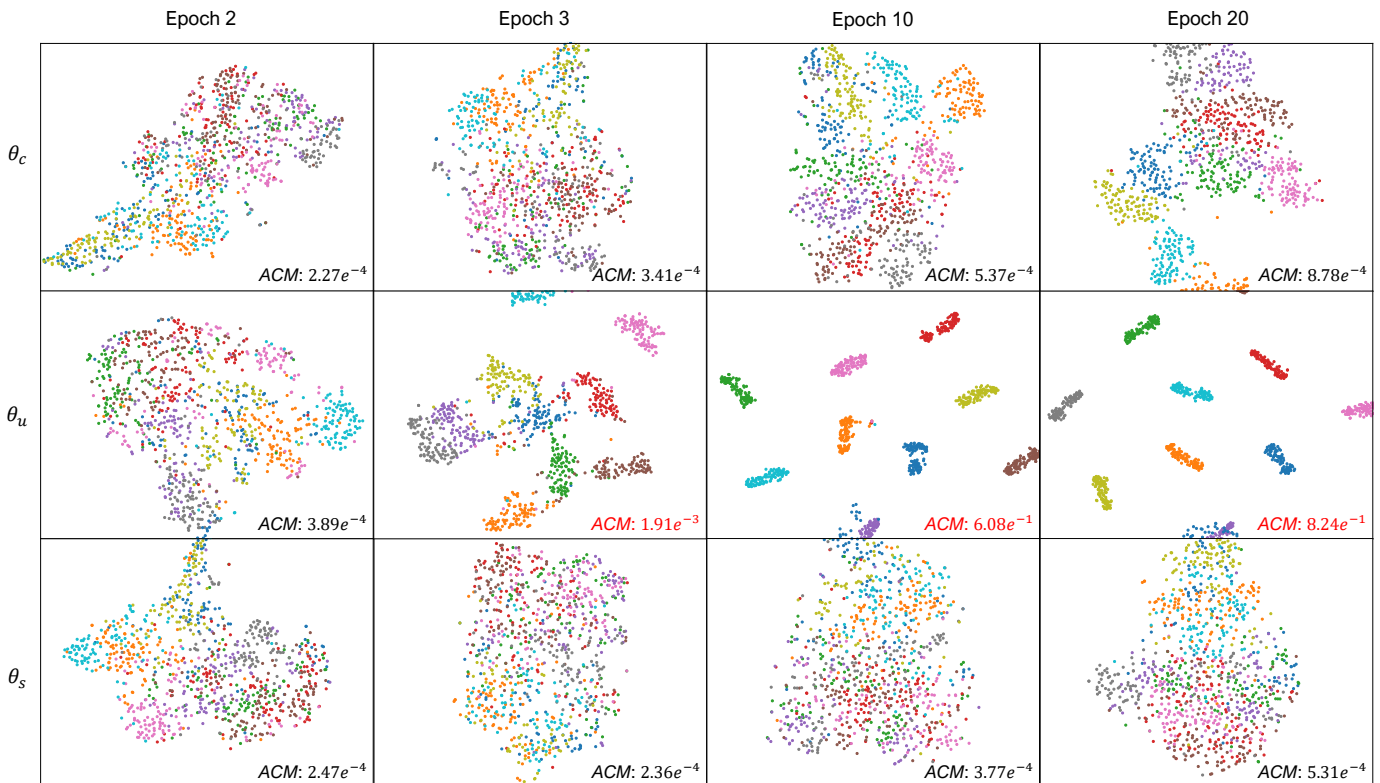


Fig. 5. The penultimate layer activation t-SNE results and ACM (Eq.(4)) of various models in different epochs. θ_c is a model naturally trained on clean data. θ_u is a model naturally trained on unlearnable data. θ_s is a model ST trained on unlearnable data. The t-SNE results and ACM of θ_s are similar to θ_c and different from θ_u , which reflects that our method ST truly prevents models from learning unlearnable perturbation features.

at a low level. However, we observe that training accuracy and test accuracy increase during the initial few epochs. This suggests that the model successfully acquires valid semantic features of the image. After the third epoch, the training accuracy increases sharply, while the test accuracy experiences a significant decline. This indicates that the model is becoming trapped in unlearnable perturbation features learning.

This insight motivates us to dynamically adjust the model’s learning process during training to reduce the chance of learning unlearnable perturbation features. To achieve this, it is first necessary to identify the point at which the model becomes trapped in learning unlearnable perturbation features. In this work, we propose (ACM) to detect this point. We train the model under the monitoring of a metric (ACM) to prevent it from being captured by unlearnable perturbation features.

We also consider whether counter-overfitting methods (such as Cutout, Mixup, Cutmix, Drop-out, Wweight-decay, Autoaugment, Gaussian-filter) [43]–[49] can effectively liberate the model from learning unlearnable perturbation features (details in Sec. IV-B2). However, these methods do not account for such powerful unlearnable perturbations and consequently, underperform in overcoming unlearnable examples.

Insight 2: Compared to deeper layers, correctly guiding the model’s shallow layers to learn image semantic features plays a crucial role in preventing the model from becoming trapped in learning unlearnable perturbation features. As shown in Fig. 3, to demonstrate such insight, we first trained a ResNet-18 [1] model on clean CIFAR-10 [16] denoted by θ_c , which achieves 92.41% accuracy on CIFAR-10 test data. Then, a

ResNet-18 was randomly initialized and the first two residual blocks were supplanted with the initial two residual blocks from θ_c . The parameters of these replaced blocks were then set to be unmodifiable. This modified model is denoted as θ_u^S . Similarly, we randomly initialized another ResNet-18 and replaced the last two residual blocks with the last two residual blocks of θ_c . Then we froze these replaced blocks’ parameters and denoted this ResNet18 by θ_u^D . Finally, we trained θ_u^S and θ_u^D on CIFAR-10 unlearnable data individually. Training results are presented in Fig. 4 (more results of other architectures and datasets can be found in Sec. IV-C1).

Our findings demonstrate that θ_u^S performs better on CIFAR-10 test data, which proves that we should concentrate on the training process of a model’s shallow layers if we aim to overcome unlearnable examples (like θ_u^S). This is because incorrect activation signals transmitted from the shallow layers can easily mislead the deeper layers, even if the deep layers themselves correctly learn image semantic features (like θ_u^D), which leads the whole model trapped in unlearnable perturbation features learning.

In this case, correctly guiding the model’s shallow layers to learn image semantic features is crucial for undermining the protective capability of unlearnable examples. This insight prompted us to implement a learning rate scheduling strategy. We gradually diminish the learning process from the shallow to the deeper layers of the model to retain the image semantic features already learned by the model and break the learning trap created by unlearnable perturbations.

Algorithm 1 Progressive Staged Training (ST)

```

1: Input: dataset  $\mathcal{D}$ , model  $f_{\theta} = \{f_{\theta_1}, f_{\theta_2}, \dots, f_{\theta_l}\}$ , subset
    $\mathcal{D}^s$ , threshold  $\gamma$ , hyperparameter  $\beta$ , epoch number  $E$ ,
   learning rate  $\eta$ , attenuation function  $Atten$ .
2: Initialize  $\tau_e \leftarrow 0$ ,  $\hat{\eta}_i^0 \leftarrow \eta$ ,  $\mathbf{H}^{tmp} \leftarrow \mathbf{H}^0 \leftarrow$ 
    $[\alpha_1^0, \alpha_2^0, \dots, \alpha_l^0] \leftarrow [1, 1, \dots, 1]$ ,  $\theta^{tmp} \leftarrow \theta$ .
3: for  $e = 1$  to  $E$  do
4:    $\hat{\eta}_i^e \leftarrow f_{Atten}(\hat{\eta}_i^{e-1})$ ,  $\eta_i^e \leftarrow \alpha_i^e \cdot \hat{\eta}_i^e$ 
5:    $\theta_i \leftarrow Train(\eta_i^e, \mathcal{D})$ 
6:   if  $f_{ACM}(\theta, \mathcal{D}^s) > \gamma$  and  $\tau^e < \frac{1}{\beta} - 1$  then
7:      $\tau^e \leftarrow \tau^e + 1$   $\triangleright$  tends to learn perturbation features
8:      $\theta \leftarrow \theta^{tmp}$   $\triangleright$  load checkpoint from  $\theta^{tmp}$ 
9:      $\mathbf{H}^e \leftarrow [\alpha_1^e, \alpha_2^e, \dots, \alpha_l^e]$   $\triangleright$  Eq. (5)
10:  else  $\triangleright$  model does not tend to learn perturbation
   features
11:    if  $\tau^e = 0$  then
12:       $\mathbf{H}^e \leftarrow [1, 1, \dots, 1]$   $\triangleright$  shift to natural training
13:    else
14:       $\mathbf{H}^e \leftarrow \mathbf{H}^{tmp}$   $\triangleright$  adjust learning rate
15:    end if
16:     $\theta^{tmp} \leftarrow \theta$   $\triangleright$  save checkpoint to  $\theta^{tmp}$ 
17:  end if
18:   $\mathbf{H}^{tmp} \leftarrow \mathbf{H}^e$ 
19: end for

```

B. ST Training Framework

In light of the aforementioned insights, we introduce Progressive Staged Training (ST), a novel strategy that gradually adjusts the learning rate of different layers, moving from shallow to deep layers, when shows a tendency to learn unlearnable perturbation features. To determine the appropriate timing for the modification of the learning rate of these layers, we propose the Activation Cluster Measurement (ACM). It serves as an indicator to identify the point at which the model becomes trapped in learning unlearnable perturbation features during the training phase. Simultaneously, we propose a novel learning rate schedule algorithm progressively curbing the shallow layers' unlearnable perturbation features learning process. A comprehensive overview of ST can be found in Fig. 2.

ACM Indicator. We propose a metric to quantitatively estimate whether the model is in a perturbation learning state, based on the observation that unlearnable perturbations construct simple features, and models are recognized to be “lazy” and prefer to learn simple unlearnable perturbation features rather than difficult image semantic features [23].

To make the above analysis clear and visualized, we present the t-SNE [50] clustering results of the penultimate layer activation at different training epochs. As shown in Fig. 5, when a model is trained on unlearnable examples, the activation cluster disorder at early epochs, i.e., the intra-class distance is large and inter-class distance is small. As training goes on, the activation begins to cluster well (a small intra-class distance and a large inter-class distance), which is a phenomenon of unlearnable perturbation features learning (other t-SNE results can be found in Sec. IV-C2). To quantify this phenomenon,

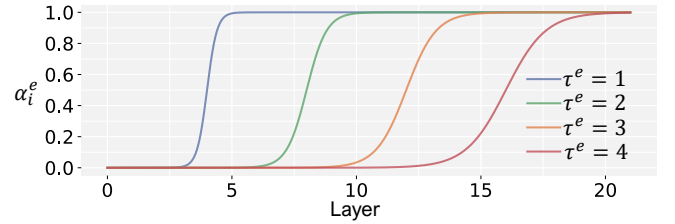


Fig. 6. Different τ^e value for α_i^e in Eq. (5) with $\beta = \frac{1}{5}$, $l = 20$. When a model trends to learn unlearnable perturbation features the value of τ^e will increase and the α_i^e of different layers will decrease, which means the learning rate of these layers will decrease gradually to terminate incorrect feature learning.

we propose a clustering measure named Activation Cluster Measurement (ACM) to describe the disorder of activation in different training epochs inspired by [27]. Suppose that $\mathcal{D} = \{\mathcal{D}_i\}_{i=1}^k$ is a dataset with k labels, and \mathcal{D}_i is the set of samples in class i . We define set \mathbf{A}_i^θ as the penultimate layer activation of model θ when given it with set \mathcal{D}_i as inputs. The cluster center of class i is defined as $\zeta(i) = \frac{1}{|\mathbf{A}_i^\theta|} \sum_{\mathbf{u} \in \mathbf{A}_i^\theta} \mathbf{u}$. Then we have the intra-class distance f_{intra} for class i as:

$$f_{intra}(i) = \frac{1}{|\mathbf{A}_i^\theta|} \sum_{\mathbf{u} \in \mathbf{A}_i^\theta} \|\mathbf{u} - \zeta(i)\|_2 \quad (2)$$

And the inter-class distance f_{inter} between class i and j is as follows:

$$f_{inter}(i, j) = \min \{\|\mathbf{u} - \mathbf{v}\|_2\}_{\mathbf{u} \in \mathbf{A}_i^\theta, \mathbf{v} \in \mathbf{A}_j^\theta} \quad (3)$$

Then we define ACM of model θ on dataset \mathcal{D} as:

$$f_{ACM}(\theta, \mathcal{D}) = \frac{1}{k(k-1)} \sum_{\substack{i, j=1 \\ i \neq j}}^k \frac{f_{inter}(i, j)}{\xi_i f_{intra}(i) + \xi_j f_{intra}(j)} \quad (4)$$

where k is the number of classes. ξ_i is the radius of class i : $\xi_i = \max \{\|\mathbf{u} - \zeta(i)\|_2\}_{\mathbf{u} \in \mathbf{A}_i^\theta}$. We use \mathcal{D}_s , a subset of the training dataset, as the validation set to calculate ACM metric during staged training. As the training progresses, the clustering of the model's activation values becomes more pronounced, with the inter-cluster distance (f_{inter}) increasing, and the intra-cluster distance (f_{intra}) decreasing, leading to a larger Activation Clustering Metric (ACM) value. By observing the ACM, we can accurately measure the extent of unlearnable perturbation features learning in the model, which is beneficial for taking steps to learn image semantic features.

Progressive Staged Training. Based on the insights, we propose progressive staged training (ST), a novel stage training framework to defeat unlearnable examples. For a given model $f_{\theta} = \{f_{\theta_1}, f_{\theta_2}, \dots, f_{\theta_l}\}$ with l layers and a dataset \mathcal{D} , the natural training (NT) process goes through three steps traditionally in each epoch: learning rate attenuation, forward propagation, and backpropagation. Differently, ST goes through five steps in each epoch: learning rate attenuation, learning rate adjustment, forward propagation, backpropagation, and ACM calculation. Once ACM indicates unlearnable perturbation features learning at the end of an epoch, the model will roll back to the checkpoint of the last epoch. Then, the learning rate will be further modified by an adjustment algorithm after learning rate attenuation to slow down the learning process of shallow layers gradually to resist the wrong learning process.

Suppose the initial learning rate of the i th layer of model θ is $\hat{\eta}_i^0$ and f_{Atten} is a learning rate attenuation function like momentum [51], cosine [52], etc. In every epoch, we first get an attenuated learning rate $\hat{\eta}_i^e = f_{Atten}(\hat{\eta}_i^{e-1})$, e for the e -th epoch. Then we get a new learning rate η_i^e by adjusting $\hat{\eta}_i^e$ with $\eta_i^e = \alpha_i^e \cdot \hat{\eta}_i^e$ (i for the i -th layer).

$$\alpha_i^e = 1 - \frac{1}{1 + e^{\frac{i}{\beta \cdot \tau^e} - l}} \quad (5)$$

where τ^e is a counter for how many time ACM larger than a threshold γ from the beginning to epoch e and β is a hyperparameter. As in Fig. 6, when a model inclines towards learning unlearnable perturbation features, the value of τ^e escalates concurrently with a reduction in the values of α_i^e across a greater number of shallow layers. This implies that the learning rate associated with these layers will gradually reduce, thereby terminating the learning of incorrect features.

The process of ST is described in Alg. 1. We use a vector $\mathbf{H}^e = [\alpha_1^e, \alpha_2^e, \dots, \alpha_l^e]$ to describe how the learning rate adjustment algorithm works and defeats unlearnable example. At the beginning of training, we init $\mathbf{H}^0 = [1, 1, \dots, 1]$ (line 2), which is equivalent to natural training, and all layers have the same learning rate. As the training goes on, the model tends to learn unlearnable perturbation features detected by ACM , and the count τ_e is increased (line 7). Subsequently, the model reverts to a previous checkpoint where it has not yet become trapped in learning unlearnable perturbation features (line 8). As τ_e increases, the α_i^e of shallow layers decreases gradually, and \mathbf{H}^e consequently logs α_i^e for each layer of the model (line 9). Following this, the next training epoch commences, with the α_i^e stored in \mathbf{H}^e adjusting the decayed learning rate (line 4). Therefore, following the components of \mathbf{H} , the learning rate of each layer gradually decreased to zero, which means the optimization gradually slowed down from shallow layers to deep layers to resist the wrong learning process.

ST Training Pipeline. We also investigate that some data augmentations, e.g., color-jitter and gray-scale (CG) [53], could promote the performance of ST (details in Sec. IV-C6). We analyze that CG makes unlearnable perturbations harder to learn for models and weaker on data protection, even if including these augmentations into the EoT process [22] of some unlearnable example generators. Furthermore, we analyze adaptive attacks that impose progressive staged training while generating perturbations (details in Sec. IV-C5). The results show that such adaptive attack perturbations are weak in data protection, and progressive staged training works well on them.

In this case, we propose the complete ST training pipeline. This involves two principal steps. In step one, we implement progressive staged training alongside augmentation CG to train a model. In step two, the model developed in step one undergoes fine-tuning aided by augmentation CG. Utilizing this ST training pipeline, we achieve state-of-the-art results to defeat unlearnable examples.

IV. EXPERIMENTS

A. Experimental Setting and Implementation

1) *Datasets and model architectures:* Three benchmarks, CIFAR-10, CIFAR-100 [16], and ImageNet-mini, a subset of

TABLE I
NOTIONS OF DIFFERENT TRAINING METHODS, WHERE NT DENOTES "NATURAL TRAINING" WHICH IS OUR BASELINE, ST DENOTES OUR "STAGED TRAINING".

	NT	NT-CG	ST	ST-CG	ST-Full
Learning rate adjustment	-	-	✓	✓	✓
Augmentation CG	×	✓	×	✓	✓
Fine-tuning with CG	-	×	×	×	✓

the first 100 classes in ImageNet [17], are used in our experiments, which is consistent with previous works of unlearnable example [22]–[24], [26]. We demonstrate the effectiveness of ST with various model architectures including ResNet-18, ResNet-50 [1], WideResNet-28-10 (WRN-28), WideResNet-34-10 (WRN-34) [54], VGG-16 [2], and DenseNet-121 [3].

2) *Unlearnable examples:* Four state-of-the-art unlearnable examples generation methods are used: Error-Minimizing perturbation (EM) [26], Robust-Error-Minimizing perturbation (REM) [22], Synthetic Perturbation (SP) [23], One-Pixel Shortcut (OPS) [24]. Meanwhile, three data poison attack generation methods are used: Adversarial Examples as Poisons (AEP) [35], Hypocritical perturbations (HYPO) [25], Autoregressive Perturbations (AP) [36]. We set the ℓ_∞ bound as $\epsilon = \frac{8}{255}$ for EM, REM, SP, AEP and ℓ_2 bound as $\epsilon = 1$ for AP, HYPO to follow their default setting. We set other hyperparameters to the default value in the open-sourced codes of EM ¹, REM ², SP ³, OPS ⁴, AEP ⁵, AP ⁶, HYPO ⁷.

3) *Baselines:* We adopt adversarial training (AT) with a bound of $\ell_\infty \leq \frac{4}{255}$ as the baseline following the REM's setting. Meanwhile, we use Ueraser ⁸ and LE ⁹ as baselines. These works primarily focus on data processing methods for learning from unlearnable samples. In contrast, our approach is orthogonal, optimizing the learning process through dynamic adjustment of the learning rate to effectively handle such samples. We set hyperparameters to the default value in their open-sourced codes.

4) *Training settings:* To show our effectiveness, we compare the natural training method with 3 different settings of ST (as summarized in Tab. I). Specifically, we implement ST with β set to 50% for CIFAR-10, ImageNet-mini, and 33.33% for CIFAR-100. Meanwhile, we set γ to 2.6×10^{-4} . We use a subset of the training dataset (unlearnable perturbation contaminated images), \mathcal{D}^s , containing 1000 samples for CIFAR-10 (each class contains 100 samples) and 5000 samples for CIFAR-100, ImageNet-mini (each class contains 50 samples) as the validation set (all the images in validation set are contaminated by unlearnable perturbation) to calculate the ACM metric during staged training. Following previous work on unlearnable examples (EM, REM, and SP), we perform random flipping on the image in all experiments. Then, we randomly crop the image to 32×32

¹<https://github.com/HanxunH/Unlearnable-Examples>

²<https://github.com/fshp971/robust-unlearnable-examples>

³<https://github.com/dayu11/Availability-Attacks-Create-Shortcuts>

⁴<https://openreview.net/forum?id=p7G8t5FVn2h>

⁵https://github.com/lhfowl/adversarial_poisons

⁶<https://github.com/psandovalsegura/autoregressive-poisoning>

⁷<https://github.com/TLMichael/Delusive-Adversary>

⁸<https://github.com/lafeat/ueraser>

⁹https://github.com/jiangw-0/LE_JCDP

TABLE II

CIFAR-10 CLEAN TEST ACCURACIES (%) AND AVERAGE RUN TIME (h) FOR NATURAL TRAINING (NT), ADVERSARIAL TRAINING (AT), UERASER, LE AND ST IN DIFFERENT VERSIONS (OURS) WITH VARIOUS MODELS ON FOUR UNLEARNABLE EXAMPLE METHODS.

	Methods	ResNet-18	ResNet-50	VGG-16	DenseNet-121	WRN-28	WRN-34	Avg. Acc.(%)	Avg. Time (h)
Clean	NT	92.41	91.78	91.57	95.04	94.68	93.69	93.20	0.76
	AT	88.23	87.96	85.32	44.03	78.18	84.01	77.96 (-15.24)	5.27
	ST	82.43	84.16	70.00	59.02	91.55	84.11	78.55 (-14.66)	2.01
	ST-CG	86.62	86.82	80.56	62.32	92.06	85.44	82.30 (-10.90)	2.31
	ST-Full	93.79	94.73	93.11	89.47	95.37	93.05	93.25 (+0.05)	3.47
EM	NT	19.93	18.89	14.88	20.25	16.79	38.26	21.50	0.71
	AT	88.62	89.28	86.28	46.02	71.67	90.05	78.65 (+57.15)	5.30
	LE	81.51	76.17	84.28	77.14	83.29	84.36	81.13 (+59.63)	2.22
	UEraser	86.11	85.59	81.76	86.12	81.56	86.44	84.60(+63.10)	1.51
	ST	58.63	78.44	69.97	56.65	37.43	79.43	63.425 (+41.93)	1.98
	ST-CG	80.18	83.43	61.52	58.11	84.56	86.56	75.73 (+54.23)	2.34
ST-Full	87.05	92.84	82.30	87.18	88.69	93.11	88.53 (+67.03)	3.61	
REM	NT	21.86	25.30	38.81	32.28	26.43	20.37	27.51	0.76
	AT	48.16	40.65	65.23	32.04	26.92	48.39	43.57(+16.06)	5.05
	LE	80.78	80.67	72.91	70.29	75.22	78.27	76.36 (+48.85)	2.65
	UEraser	67.48	78.18	71.59	71.91	61.75	61.43	68.78 (+41.27)	1.62
	ST	82.11	68.90	57.13	41.23	39.84	81.25	61.74 (+34.23)	2.00
	ST-CG	77.08	79.02	61.03	43.56	76.16	83.04	69.98 (+42.47)	2.01
ST-Full	78.86	85.86	74.43	72.94	74.23	84.01	78.39 (+50.88)	3.17	
SP	NT	13.67	15.85	16.40	25.83	14.31	12.95	16.50	0.78
	AT	22.21	52.02	61.12	47.63	58.26	64.41	50.94 (+34.44)	5.27
	LE	82.94	86.78	83.78	76.73	83.27	81.48	82.50 (+66.00)	2.19
	UEraser	80.58	85.57	84.56	75.45	85.65	83.47	82.55 (+66.05)	1.62
	ST	42.73	39.43	53.31	50.59	37.25	42.04	44.23 (+27.73)	1.84
	ST-CG	66.75	77.19	79.43	55.36	86.32	79.82	74.15 (+57.65)	1.86
ST-Full	79.69	83.75	86.13	73.15	87.25	85.47	82.57 (+66.07)	2.98	
OPS	NT	21.71	19.20	17.25	25.01	31.67	19.69	22.42	0.82
	AT	21.08	15.20	18.6	32.14	48.19	47.75	30.49 (+8.07)	5.06
	LE	75.59	71.91	63.16	65.47	71.22	76.91	70.71 (+48.29)	2.51
	UEraser	69.75	68.40	56.95	68.15	61.68	68.76	65.62 (+43.20)	1.68
	ST	53.25	57.18	44.66	55.02	41.45	73.55	54.19 (+31.77)	1.87
	ST-CG	75.58	80.37	65.45	58.06	64.84	81.34	70.94 (+48.52)	1.92
ST-Full	76.19	80.93	57.16	45.13	64.79	81.86	67.68 (+45.26)	3.06	
AEP	NT	6.82	9.17	13.08	22.43	13.91	9.78	12.53	0.74
	AT	73.84	71.26	58.68	38.88	74.81	76.95	65.74 (+53.21)	5.31
	LE	73.22	74.62	60.27	48.65	59.83	62.76	63.23 (+50.70)	2.47
	UEraser	51.13	44.97	39.37	52.52	66.83	49.72	50.76 (+38.23)	1.49
	ST	82.48	72.81	64.56	55.53	45.71	72.29	65.56 (+53.03)	1.78
	ST-CG	84.45	82.94	62.64	55.27	62.28	84.25	71.97 (+59.44)	1.81
ST-Full	85.08	83.31	51.38	46.63	60.15	84.72	68.55 (+56.01)	3.11	
AP	NT	18.43	17.21	16.86	33.06	12.78	10.44	18.13	0.72
	AT	60.13	57.21	11.21	18.67	73.65	74.58	49.24 (+31.11)	5.21
	LE	78.61	81.03	75.24	71.83	75.01	76.25	76.33 (+58.20)	2.52
	UEraser	74.22	71.51	75.58	75.13	76.38	72.63	74.24 (+56.11)	1.60
	ST	82.11	81.51	69.62	57.81	59.46	87.08	72.93 (+54.80)	1.88
	ST-CG	86.77	85.79	72.15	57.59	87.18	85.63	79.19 (+61.06)	1.91
ST-Full	87.51	86.62	77.91	65.44	88.21	86.79	82.08 (+63.95)	3.31	
HYPO	NT	12.34	13.15	16.64	19.23	10.11	10.39	13.64	0.73
	AT	17.11	15.61	10.12	14.93	13.29	15.93	14.50 (+0.86)	5.30
	LE	67.57	70.88	60.81	66.72	68.57	69.17	67.29 (+53.65)	2.22
	UEraser	58.94	58.71	65.84	64.69	68.05	51.19	61.24 (+47.60)	1.68
	ST	81.75	59.28	50.13	49.30	38.51	82.11	60.18 (+46.54)	1.94
	ST-CG	73.09	78.12	50.30	48.73	66.84	85.55	67.11 (+53.47)	2.04
ST-Full	73.19	79.36	55.46	41.46	68.88	86.05	67.40 (+53.76)	3.31	

size for CIFAR-10 and CIFAR-100 and 224×224 size for ImageNet-mini.

For normal training (NT), we use the SGD optimizer accompanied by the cosine learning rate decay, with momentum set to 0.9, weight decay set to 10^{-4} , and learning rate set to 0.1. For adversarial training (AT), we use the SGD optimizer accompanied by the cosine learning rate decay, with momentum set to 0.9, weight decay set to 10^{-4} , and learning rate set to 0.1. For the ST series (ours), we use the SGD optimizer accompanied by the cosine learning rate decay, with momentum set to 0.9, weight decay set to 10^{-4} , and learning rate set to 0.1 for ST and 0.2 for ST-CG. In the ACM calculation stage, we reduced the activation of the penultimate layer to two dimensions with t-SNE. Meanwhile, we use the first

ten classes to calculate ACM for CIFAR-10 and ImageNet-mini. Following traditional data augmentation methods in deep learning, we perform color-jitter on images with 80% probability and gray-scale with 20% probability. For fine-tuning with CG, we fine-tune all layers of a model and use the SGD optimizer accompanied by the cosine learning rate decay, with momentum set to 0.9, and weight decay set to 10^{-4} . In the absence of specific clarification, EM refers to EM sample-wise perturbation. All experiments are conducted on 8 GPU (NVIDIA[®] Tesla[®] A100[®]).

B. Learning Effectiveness.

1) *Experimental Result:* Tab. II shows the clean test accuracy of models on CIFAR-10 after being protected with

TABLE III

CIFAR-100 CLEAN TEST ACCURACIES (%) FOR NATURAL TRAINING (NT), ADVERSARIAL TRAINING (AT), UERASER, LE AND ST IN DIFFERENT VERSIONS (OURS) WITH VARIOUS MODELS ON FOUR UNLEARNABLE EXAMPLE METHODS.

Methods	Frame	ResNet-18	ResNet-50	VGG-16	DenseNet-121	WRN-28	WRN-34	Average
Clean	NT	70.77	73.69	67.27	61.99	77.31	71.28	70.38
	AT	61.50	65.81	56.59	28.23	48.72	64.01	54.14(-16.24)
	ST	49.57	55.70	41.50	30.18	66.86	61.37	50.86 (-19.52)
	ST-CG	52.31	58.68	39.22	36.22	65.23	59.84	51.92 (-18.46)
	ST-Full	71.84	73.11	70.83	61.76	75.08	72.11	70.78 (+0.41)
EM	NT	14.81	12.19	22.18	13.71	14.48	28.20	17.60
	AT	64.17	66.43	56.96	26.51	46.15	68.27	54.75 (+37.15)
	LE	53.72	51.89	52.59	53.36	61.23	55.56	54.73 (+37.13)
	UEraser	57.27	56.81	56.91	56.43	50.61	56.25	55.71 (+38.11)
	ST	47.55	57.56	38.13	32.13	51.27	59.34	47.66 (+30.06)
	ST-CG	51.93	54.91	40.59	41.05	65.01	61.30	52.47 (+34.87)
REM	NT	8.71	17.28	13.51	16.04	8.83	10.65	12.50
	AT	27.10	26.03	48.85	21.18	39.25	25.04	31.24 (+18.74)
	LE	50.21	53.86	50.91	50.38	52.88	50.29	51.42 (+38.92)
	UEraser	50.84	55.04	49.13	48.22	54.96	52.05	51.71 (+39.21)
	ST	47.61	35.52	29.81	24.33	27.54	36.29	33.52 (+21.02)
	ST-CG	52.94	49.45	23.92	25.35	61.11	57.02	44.97 (+32.47)
SP	NT	9.54	8.51	10.57	9.45	11.13	10.36	9.93
	AT	24.81	29.84	28.71	23.19	39.11	43.09	31.46 (+21.53)
	LE	53.19	55.27	61.74	51.89	56.29	54.71	55.52 (+45.59)
	UEraser	51.18	55.11	56.16	50.03	56.73	53.61	53.80 (+43.87)
	ST	32.54	27.12	28.84	28.73	27.82	26.35	28.57 (+18.64)
	ST-CG	48.03	48.98	37.66	34.75	54.90	46.70	45.17 (+35.24)
OPS	NT	13.93	12.21	8.90	12.85	14.55	11.34	12.30
	AT	10.85	17.07	10.17	11.15	21.86	24.82	15.99 (+3.69)
	LE	44.22	40.71	33.01	36.38	43.36	41.93	39.94 (+27.64)
	UEraser	32.77	31.56	32.63	31.67	32.29	32.45	32.23 (+19.93)
	ST	29.98	51.79	36.55	29.85	32.76	56.84	39.63 (+27.32)
	ST-CG	47.73	56.53	34.81	33.75	50.34	57.44	46.77 (+34.47)
ST-Full	NT	13.93	12.21	8.90	12.85	14.55	11.34	12.30
	AT	10.85	17.07	10.17	11.15	21.86	24.82	15.99 (+3.69)
	LE	44.22	40.71	33.01	36.38	43.36	41.93	39.94 (+27.64)
	UEraser	32.77	31.56	32.63	31.67	32.29	32.45	32.23 (+19.93)
	ST	29.98	51.79	36.55	29.85	32.76	56.84	39.63 (+27.32)
	ST-CG	47.73	56.53	34.81	33.75	50.34	57.44	46.77 (+34.47)
ST-Full	NT	13.93	12.21	8.90	12.85	14.55	11.34	12.30
	AT	10.85	17.07	10.17	11.15	21.86	24.82	15.99 (+3.69)
	LE	44.22	40.71	33.01	36.38	43.36	41.93	39.94 (+27.64)
	UEraser	32.77	31.56	32.63	31.67	32.29	32.45	32.23 (+19.93)
	ST	29.98	51.79	36.55	29.85	32.76	56.84	39.63 (+27.32)
	ST-CG	47.73	56.53	34.81	33.75	50.34	57.44	46.77 (+34.47)
ST-Full	NT	13.93	12.21	8.90	12.85	14.55	11.34	12.30
	AT	10.85	17.07	10.17	11.15	21.86	24.82	15.99 (+3.69)
	LE	44.22	40.71	33.01	36.38	43.36	41.93	39.94 (+27.64)
	UEraser	32.77	31.56	32.63	31.67	32.29	32.45	32.23 (+19.93)
	ST	29.98	51.79	36.55	29.85	32.76	56.84	39.63 (+27.32)
	ST-CG	47.73	56.53	34.81	33.75	50.34	57.44	46.77 (+34.47)
ST-Full	NT	13.93	12.21	8.90	12.85	14.55	11.34	12.30
	AT	10.85	17.07	10.17	11.15	21.86	24.82	15.99 (+3.69)
	LE	44.22	40.71	33.01	36.38	43.36	41.93	39.94 (+27.64)
	UEraser	32.77	31.56	32.63	31.67	32.29	32.45	32.23 (+19.93)
	ST	29.98	51.79	36.55	29.85	32.76	56.84	39.63 (+27.32)
	ST-CG	47.73	56.53	34.81	33.75	50.34	57.44	46.77 (+34.47)
ST-Full	NT	13.93	12.21	8.90	12.85	14.55	11.34	12.30
	AT	10.85	17.07	10.17	11.15	21.86	24.82	15.99 (+3.69)
	LE	44.22	40.71	33.01	36.38	43.36	41.93	39.94 (+27.64)
	UEraser	32.77	31.56	32.63	31.67	32.29	32.45	32.23 (+19.93)
	ST	29.98	51.79	36.55	29.85	32.76	56.84	39.63 (+27.32)
	ST-CG	47.73	56.53	34.81	33.75	50.34	57.44	46.77 (+34.47)
ST-Full	NT	13.93	12.21	8.90	12.85	14.55	11.34	12.30
	AT	10.85	17.07	10.17	11.15	21.86	24.82	15.99 (+3.69)
	LE	44.22	40.71	33.01	36.38	43.36	41.93	39.94 (+27.64)
	UEraser	32.77	31.56	32.63	31.67	32.29	32.45	32.23 (+19.93)
	ST	29.98	51.79	36.55	29.85	32.76	56.84	39.63 (+27.32)
	ST-CG	47.73	56.53	34.81	33.75	50.34	57.44	46.77 (+34.47)

TABLE IV

IMAGENET-MINI CLEAN TEST ACCURACIES (%) FOR NATURAL TRAINING (NT), ADVERSARIAL TRAINING (AT), AND OUR ST IN DIFFERENT SETTINGS OVER VARIOUS UNLEARNABLE EXAMPLE METHODS ON RESNET-18 AND DENSENET-121.

Methods	Arch.	Clean	EM	REM	SP
NT	ResNet	80.66	14.81	13.74	11.10
	DenseNet	80.27	6.58	18.51	12.58
AT	ResNet	65.73	50.05	50.43	52.05
	DenseNet	54.25	37.15	38.63	38.29
ST	ResNet	77.36	43.27	47.5	75.59
	DenseNet	65.79	65.26	48.97	65.47
ST-CG	ResNet	78.93	45.81	71.29	76.47
	DenseNet	69.86	64.4	59.69	68.37
ST-Full	ResNet	82.50	40.54	72.18	79.36
	DenseNet	80.27	68.19	68.95	79.81
ST-Full	ResNet	+1.84	+25.73	+58.44	+68.26
	DenseNet	+1.02	+61.61	+50.44	+67.23

different methods. As a pioneering method, EM perturbations have limited data protection capabilities, while methods on improving it like REM and OPS show that the natural training method cannot work well on perturbed data, most of which are less than 30% on CIFAR-10. Adversarial training (AT) works well on EM perturbations. However, AT is still less effective compared with our ST training pipeline. Especially, ST-Full

TABLE V

CIFAR-10 TEST ACCURACY (%) OF DIFFERENT COUNTER-OVERFITTING METHODS. WD FOR WEIGHT-DECAY. AA FOR AUTO-AUGMENT. RA FOR RAND-AUGMENT. GF FOR GAUSSIAN-FILTER.

Methods	Cutout [45]	Mixup [46]	Cutmix [47]	AA [48]
Test Acc.	21.66	11.24	10.34	28.12
Methods	RA [49]	GF	Dropout [43]	WD [44] (10^{-4})
Test Acc.	27.45	15.95	25.08	23.51
Methods	WD (10^{-3})	WD (10^{-2})	ℓ_∞ AT	ST
Test Acc.	21.99	21.71	48.16	82.11

trained ResNet-50 gets 92.84% on EM perturbed CIFAR-10. Meanwhile, the ST training pipeline works effectively on clean data as well as normal training indicating our method can be an add-on to the NT whether the training data is protected or not.

Tab. III shows the clean test accuracy of models on CIFAR-100 after being trained with different methods on the perturbed training data. As a pioneering method, EM perturbations have limited data protection capabilities, while methods on improving it like REM and OPS show that the natural training method cannot work well on perturbed data, most of which are less than 17% on CIFAR-100. Adversarial training (AT) works well on EM and SP perturbations. However, AT is still trivial compared with our ST training pipeline. Especially, ST-Full

TABLE VI
RESNET-18 TEST ACCURACIES (%) FOR NT AND ST TRAINED ON
PERTURBED CIFAR-10 WITH DIFFERENT PROTECTION PERCENTAGES
(RATIO).

	Ratio	0	0.2	0.4	0.6	0.8	1
EM	NT	92.41	93.12	92.04	90.72	83.90	19.93
	ST	82.43	73.70	71.23	72.18	72.54	58.63
	ST-CG	86.69	77.00	73.65	76.55	76.45	80.18
	ST-Full	93.79	93.93	93.70	92.82	92.86	87.05
REM	NT	92.41	92.15	91.75	89.29	84.65	21.86
	ST	82.43	82.52	82.61	82.79	82.65	82.11
	ST-CG	86.69	85.36	84.68	84.22	82.93	77.08
	ST-Full	93.79	81.04	78.11	79.97	78.92	78.86
SP	NT	92.41	93.09	91.50	90.11	85.19	13.67
	ST	82.43	79.22	70.95	69.86	64.97	42.73
	ST-CG	86.69	76.00	74.83	73.90	72.04	66.75
	ST-Full	93.79	93.86	93.32	93.06	91.97	79.69
OPS	NT	92.41	82.45	88.26	89.68	92.02	21.71
	ST	82.43	83.11	88.94	91.57	91.06	81.75
	ST-CG	86.69	84.09	89.20	91.02	87.79	73.09
	ST-Full	93.79	85.15	90.25	92.19	92.79	73.19

TABLE VII
RESNET-18 TEST ACCURACIES (%) FOR NT AND ST TRAINED ON
PERTURBED CIFAR-100 WITH DIFFERENT PROTECTION PERCENTAGES
(RATIO).

	Ratio	0	0.2	0.4	0.6	0.8	1
EM	NT	70.77	73.83	73.26	67.29	56.38	14.81
	ST	49.57	49.43	48.48	48.34	48.04	47.55
	ST-CG	52.31	51.89	52.12	50.93	52.00	51.93
	ST-Full	71.84	71.54	72.38	71.51	70.12	64.81
REM	NT	70.77	72.75	68.91	63.81	53.57	8.71
	ST	49.57	49.41	48.02	48.49	47.65	47.61
	ST-CG	52.31	51.62	50.31	52.73	51.53	52.94
	ST-Full	71.84	56.36	55.72	54.26	55.32	54.19
SP	NT	70.77	73.68	71.37	67.55	57.88	9.54
	ST	49.57	47.07	43.77	40.84	37.50	32.54
	ST-CG	86.69	76.00	74.83	73.90	72.04	66.75
	ST-Full	71.84	71.97	70.06	71.48	68.98	52.46
OPS	NT	70.77	41.09	58.93	64.94	69.93	13.93
	ST	49.57	42.15	59.06	60.19	53.12	29.98
	ST-CG	52.31	50.18	59.75	66.18	57.57	47.73
	ST-Full	71.84	51.47	60.93	67.25	68.43	46.73

trained ResNet-50 gets 71.94% on EM perturbed CIFAR-100. Meanwhile, the ST training pipeline works effectively on clean data as well as normal training.

Furthermore, to confirm the effectiveness of high-resolution images, we implement the ST training pipeline on ImageNet-mini. As shown in Tab. IV, ST works well on four perturbed data (especially, ST improves ResNet-18 from 11.10% to 75.59% on SP and DenseNet-121 from 6.58% to 65.26% on EM). CG augmentation supplements the performance of ST, which ST-CG achieves a good boost to ST. Meanwhile, ST-Full works perfectly on REM and SP perturbation. However, it has a decreased accuracy on EM with ResNet-18. This is because the protection of perturbation on high-resolution images is much stronger. For example, NT trained ResNet-18 on EM perturbations can achieve 19.93% accuracy in Tab. II while it decreases to 14.81% for ImageNet-mini in Tab. IV.

2) Comparison with general counter-overfitting methods.:

To investigate whether counter-overfitting methods can correctly guide the model to escape from unlearnable perturbation feature learning, we tested several counter-overfitting methods. As shown in Tab. V, we naturally trained a ResNet-18 on REM-perturbed CIFAR-10. The data augmentations, including Cutout, Mixup, Cutmix, Auto-augment, Rand-augment, and Gaussian filter, ineffectively resist unlearnable examples. Then, we implement dropout (0.5 probability) and weight-decay (WD)

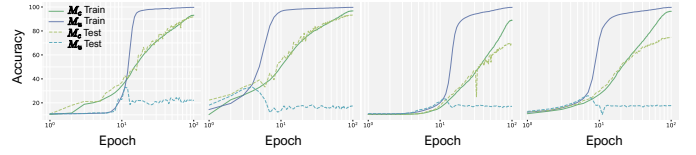


Fig. 7. From left to right, the sequence is as follows: the training and test accuracy of a ResNet-50 trained on clean CIFAR-10 (θ_c) and REM perturbed CIFAR-10 (θ_u), the training and test accuracy of a WRN34-10 trained on clean CIFAR-10 (θ_c) and perturbed CIFAR-10 (θ_u), the training and test accuracy of a ResNet-50 trained on clean CIFAR-100 (θ_c) and REM perturbed CIFAR-100 (θ_u), the training and test accuracy of a WRN34-10 trained on clean CIFAR-100 (θ_c) and perturbed CIFAR-100 (θ_u).

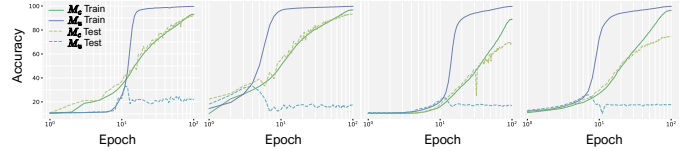


Fig. 8. From left to right, the sequence is as follows: the training and test accuracy of θ_u^S (green) and θ_u^D (blue) with VGG-16 on REM perturbed CIFAR-10, the training and test accuracy of θ_u^S (green) and θ_u^D (blue) with WRN34-10 on REM perturbed CIFAR-10, the training and test accuracy of θ_u^S (green) and θ_u^D (blue) with VGG-16 on REM perturbed CIFAR-100, the training and test accuracy of θ_u^S (green) and θ_u^D (blue) with VGG-16 on REM perturbed CIFAR-100.

from 10^{-4} to 10^{-2} , both of which cannot defeat unlearnable examples. Finally, we use adversarial training (AT) with $\ell_\infty \leq \frac{4}{255}$. ST emerges as the most effective strategy for overcoming unlearnable examples, whereas traditional counter-overfitting methods fail to systematically handle training processes.

3) Different protection percentages.: A more realistic learning scenario is that only a part of the data is protected by the defensive noise and the others are clean. We used various unlearnable methods to perturb CIFAR-10 and CIFAR-100 with different mixing ratios. The protection percentage (ratio in Tab. VI and Tab VII) represents the proportion of unlearnable examples to all samples. As shown in Tab VI and Tab VII, ST-Full has exceptional performance on all protection percentages (especially on protection percentage 1.0), which reflects the reliability of our method on mixed samples.

C. Analysis and Ablation Study

1) Observations for insights: We provide additional experiments to support our observations, including various architectures and datasets.

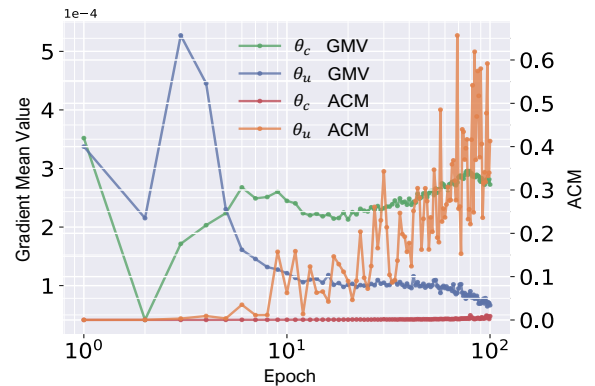


Fig. 9. (c) The mean value of gradient (GMV) of a shallow layer and ACM at each epoch when trained on clean data θ_c and unlearnable data θ_u .

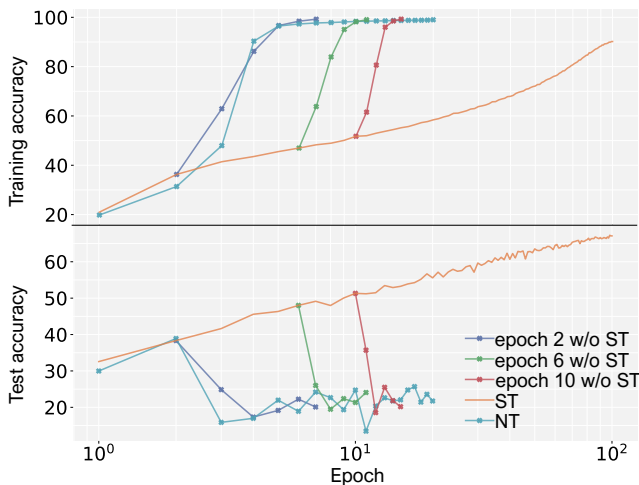


Fig. 10. The training and test accuracy of a ResNet-18 ST trained on REM perturbed data (orange), and the accuracy of not implementing ST (blue, green, red). The model will drop to an unlearnable perturbation feature learning trap without ST. NT (same as θ_u in Fig. 4) is a ResNet-18 normal trained on REM perturbed data (light blue)

Observations for Insight 1. We also show the learning process of a ResNet-50 and a WRN34-10 separately on unlearnable CIFAR-10 and CIFAR-100 in Fig. 7. Both the training accuracy and test accuracy increase at the first several epochs, indicating that the model learned the correct image features. However, as training goes on, the training accuracy increases sharply, while the test accuracy significantly decreases, indicating the model is trapped in the perturbation feature learning. These observations provide direct evidence for our insight 1.

Observations for Insight 2. We also show the learning process of a ResNet-50 and a WRN34-10 separately on unlearnable CIFAR-10 and CIFAR-100. As shown in Fig. 8, θ_u^S performs better test data, which proves that shallow layers are capable of learning the correct features at the beginning of the training (like θ_u^S). However, when shallow layers are trapped in unlearnable perturbation feature learning, even if deep layers are in the right state (like θ_u^D), shallow layers will pass the wrong activation and corrupt deep layers to a wrong learning way. These observations provide direct evidence for our insight 2.

2) *ACM Analysis:* We natural trained a ResNet-18 on clean data (θ_c) and unlearnable data (θ_u), and compare them with a ResNet-18 ST trained on unlearnable data (θ_s). Then we drew the t-SNE cluster results of the output activation of the fourth residual block layer (Fig. 11) and the sixth residual block layer (Fig. 13) of ResNet-18. The results show that when a raw model is trained on unlearnable data, the activation cluster disorder at early epochs. As training goes by, the model begins to cluster well, which is a phenomenon of unlearnable perturbation feature learning. The visualization results of t-SNE also reflect the wrong learning process during training.

The *ACM* of the model trained on clean data (θ_c) and unlearnable data (θ_u) at different training epochs is shown in Fig. 9. The *ACM* of the θ_u is low at the beginning, then it goes to a high level, which is consistent with our previous observation in t-SNE cluster results that the inter-class distance becomes larger and intra-class distance becomes

smaller. Meanwhile, The gradient mean value (GMV) of the model trained on unlearnable data falls to a low level rapidly, which illustrates that shallow layers are trapped in unlearnable perturbation feature learning and hardly learn image semantic features at late epochs compared to the model trained on clean data.

3) *ST helps to learn image semantic features:* We further illustrate how the ST framework helps to avoid unlearnable perturbation feature learning. We first train a model on REM perturbed data. When this model tends to learn unlearnable perturbation feature ($ACM > \gamma$), we either keep ST training (orange lines in Fig. 10) or shift to natural training (blue, green, red lines in Fig. 10). It demonstrates that without our learning rate adjustment algorithm, the model will fall back to unlearnable perturbation feature learning as natural training, which shows the necessity of learning rate adjustment.

To verify the effectiveness of ST, we analyze the channel-wise activation of different layers. We natural trained a ResNet-18 model separately on clean data (θ_c) and REM perturbed data (θ_u). Then we ST trained a ResNet-18 on REM perturbed data (θ_s). We analyze the channel-wise mean value of output activation from the shallow layers to the deep layers of model θ_c , θ_u and θ_s , then feed them with clean data. As shown in Fig. 12, the activation distribution of θ_s is similar with θ_c , while the activation distribution of θ_u is largely different with θ_c and θ_s . In this case, ST resists unlearnable perturbation feature learning and correctly leads the model to learn image semantic features.

4) *Hyperparameter analysis.:* We analyzed the sensitivity of hyperparameter γ and β shown in Fig. 14. 2.6×10^{-4} is a suitable value for γ . Meanwhile, $\beta = 50\%$ is a suitable value for CIFAR-10, ImageNet-mini, and $\beta = 33.33\%$ is suitable for CIFAR-100. Especially, we analyzed the sensitivity of hyperparameter γ and β on a validation set containing only 20 clean samples of the test dataset, and results show that 20 clean samples are sufficient for picking a suitable hyperparameter. In this case, while deploying our method, the engineer could collect a small validation set (only 20 samples) and pick suitable hyperparameters.

5) *Adaptive Attack: Our method works well even if CG becomes a white box setting while generating perturbation.* We propose composite data augmentation strategies to improve the learning effectiveness of unlearnable examples. In this subsection, we analyze that the CG-transformed image data lowers the chance of unlearnable perturbation feature learning. Such composite data augmentation can work effectively even if the augmentation strategy is white-box during generating unlearnable examples because it is hard to build effective unlearnable examples with more complex perturbation feature space. Suppose we have a dataset consisting of original clean examples $\mathcal{D}_{clean} = \{(\mathbf{x}_i, y_i)\}_{i=1}^n$ drawn from a distribution \mathcal{S} , where $\mathbf{x}_i \in \mathcal{X}$ is an input image and $y_i \in \mathcal{Y}$ is the associated label. We assume that the unauthorized parties will use the published training dataset to train a classifier $f_\theta : \mathcal{X} \rightarrow \mathcal{Y}$ with parameter θ . We implement augmentation CG while generating EM and EM class-wise perturbations, and we denote these perturbations by EM-T and EM-Class-T which generate as

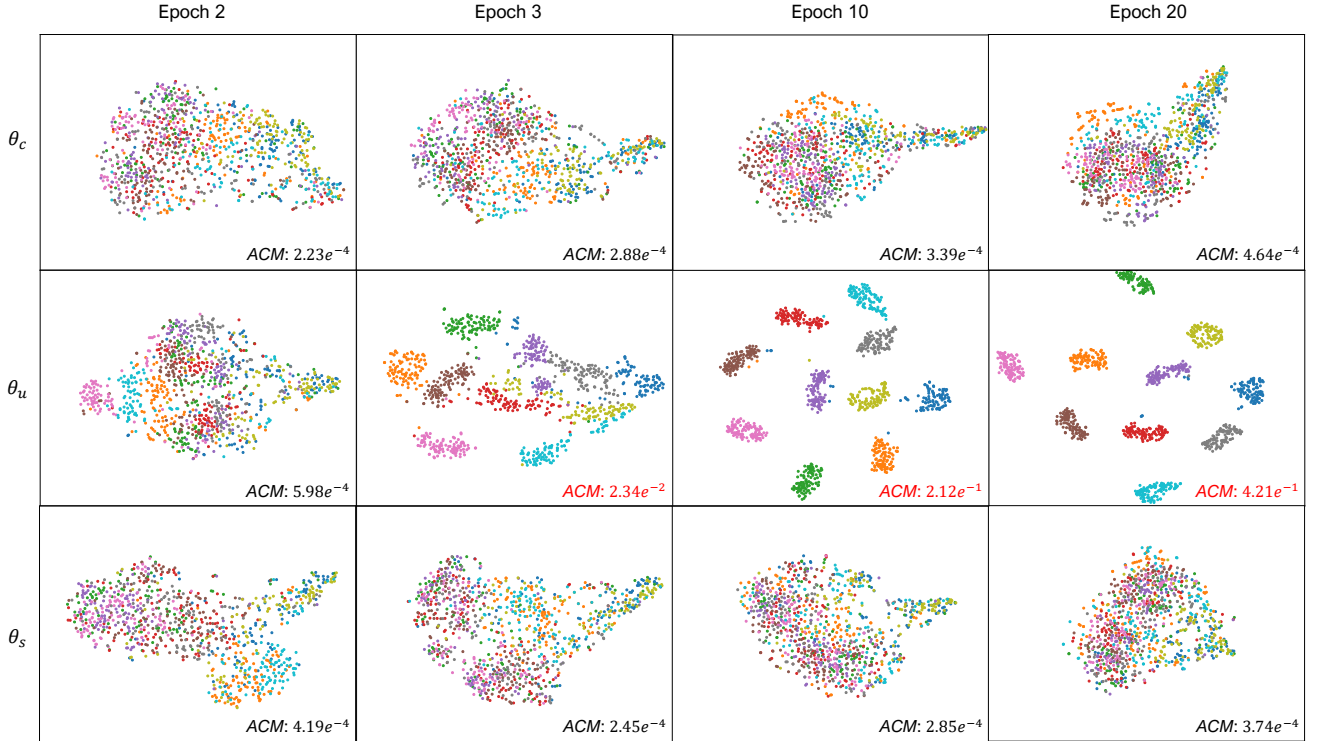


Fig. 11. The fourth residual block layer activation t-SNE results and ACM (Eq.(4)) of various models in different epochs. θ_c is a model naturally trained on clean data. θ_u is a model naturally trained on unlearnable data. θ_s is a model ST trained on unlearnable data.

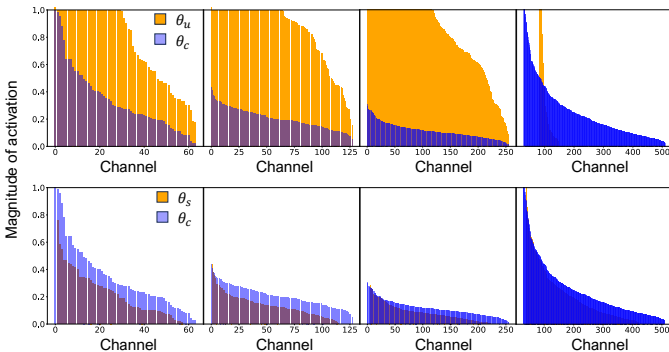


Fig. 12. The first row of images are the channel-wise mean value of output activation from the shallow layers to the deep layers of model θ_c and θ_u , while the second row of images is the channel-wise mean value of output activation from the shallow layers to the deep layers of model θ_c and θ_s . The first, second, and third columns correspond to the output activation distribution of the 2nd, 4th, and 6th residual block layers, respectively. The fourth column is the output activation distribution of the residual block layer before the full connection layer.

follows:

$$\arg \min_{\theta} \mathbb{E}_{(x_i, y_i)} \left[\min_{\delta_i} \mathcal{L}(f_{\theta}(\mathcal{T}(x_i + \delta_i)), y_i) \right] \quad (6)$$

where $\|\delta_i\|_{\infty} < \epsilon_u$, $\mathcal{T}(\cdot)$ is the augmentation CG and \mathcal{L} is the loss function. Meanwhile, We implement augmentation CG while generating REM perturbations, and we denote these perturbations by REM-T which generate as follows:

$$\arg \min_{\theta} \mathbb{E}_{(x_i, y_i)} \left[\min_{\delta_i} \max_{\sigma_i} \mathcal{L}(f_{\theta}(\mathcal{T}(x_i + \delta_i + \sigma_i)), y_i) \right] \quad (7)$$

where $\|\sigma_i\|_{\infty} < \epsilon_a$, $\|\delta_i\|_{\infty} < \epsilon_u$, $\mathcal{T}(\cdot)$ is the augmentation CG and \mathcal{L} is the loss function. Following Eq. 6 and Eq. 7, we

set CG as a white box set. As shown in Tab. VIII, our method works well with EM-T, EM-Class-T, and REM-T.

Our method works well even if ST becomes a white box setting while generating perturbation. We implement ST while generating EM, EM-Class, and REM perturbations. We denote these perturbations by EM-A, EM-Class-A, and REM-A. Meanwhile, we set augmentation CG and ST as white box settings while generating EM, EM-Class, and REM perturbations, and we denote these perturbations by EM-AT, EM-Class-AT, and REM-AT. As shown in Tab. VIII, such white-box settings will not contribute to data protection capabilities indicating the effectiveness of our method.

TABLE VIII

CIFAR-10 CLEAN TEST ACCURACIES (%) FOR NATURAL TRAINING (NT), NATURAL TRAINING WITH AUGMENT CG (NT-CG) AND ST IN DIFFERENT VERSIONS (OURS) WITH RESNET18 ON CLEAN SAMPLES AND VARIOUS UNLEARNABLE EXAMPLES. EM IS FOR SAMPLE-WISE EM PERTURBATIONS AND EM-CLASS IS FOR CLASS-WISE EM PERTURBATIONS.

Method	NT	NT-CG	ST	ST-CG	ST-Full
Clean	92.41	93.20	82.43	86.62	93.79
EM	19.93	60.03	58.63	78.44	87.05
EM-T	23.19	80.30	68.23	78.47	81.19
EM-A	91.57	92.86	69.33	69.79	93.48
EM-AT	93.29	93.01	71.18	76.13	93.54
EM-Class	9.39	34.22	46.29	71.08	80.04
EM-Class-T	17.05	77.7	55.96	65.72	76.08
EM-Class-A	92.80	93.12	69.66	73.16	93.63
EM-Class-AT	76.43	92.81	68.15	73.79	85.87
REM	21.86	55.62	82.11	77.08	78.86
REM-T	61.03	72.36	65.06	68.15	78.34
REM-A	35.22	81.84	54.59	64.47	84.93
REM-AT	60.13	79.93	55.52	65.72	81.81

6) *Data Augmentation.* : To verify the effectiveness of color-jitter and gray-scale (CG). Color jitter randomly changes an image's brightness, contrast, saturation, and hue. Gray-scale

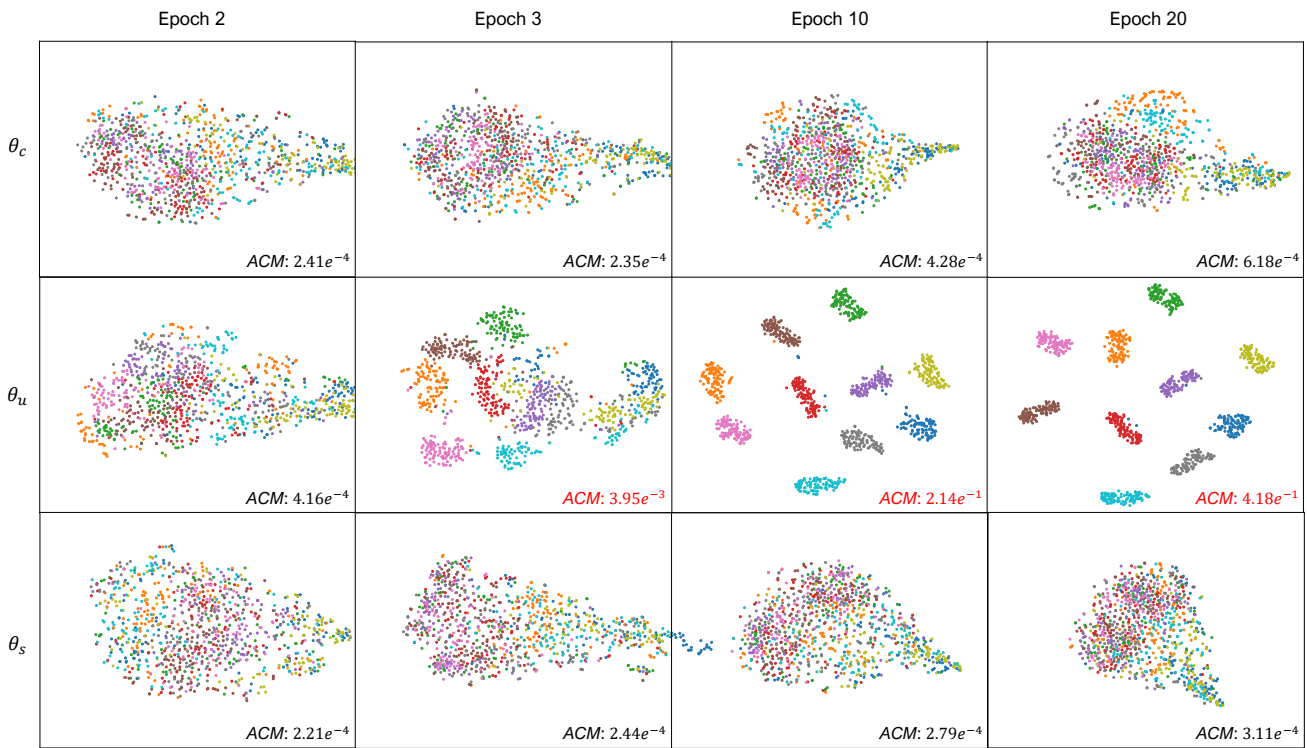


Fig. 13. The sixth residual block layer activation t-SNE results and ACM (Eq.(4)) of various models in different epochs. θ_c is a model naturally trained on clean data. θ_u is a model naturally trained on unlearnable data. θ_s is a model ST trained on unlearnable data.

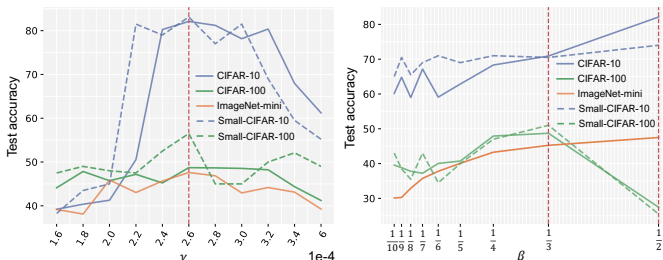


Fig. 14. *Left*: The test accuracy of a ResNet-18 ST-CG trained on REM perturbed data. *Right*: The test accuracy of a ResNet-18 ST-CG trained on REM perturbed data.

randomly converts an image to grayscale. We have conducted experiments on REM perturbed CIFAR-10 using various data augmentations on ResNet-18, and the results indicate that not all data augmentations can break unlearnable perturbations (Table IX). In this case, we utilized CG as an auxiliary means to enhance the performance of ST.

TABLE IX

TEST ACCURACY (%) OF NORMAL TRAINED RESNET-18 ON REM PERTURBED CIFAR-10 WITH VARIOUS AUGMENTATIONS.

Methods	Mixup	Cutmix	Gamma	Brightness	Solarize
Test Acc.	11.24	10.34	17.76	20.46	22.92
Methods	Hue	Grayscale	Colorjitter	NT-CG	ST
Test Acc.	18.71	45.62	37.21	55.62	82.11

7) *Comparison with defensive measures against data poisoning attacks.* : Currently, there is a lack of methods to counteract unlearnable examples that can be compared with our approach ST, while data poison attacks share the same principle with unlearnable examples. In this case, we verified the efficiency of different defensive measures against data poisoning attacks [55], [56] with a ResNet-18 on EM, REM, SP perturbed CIFAR-10 in Tab. X. The results indicate that the defensive measures against data poisoning attacks are ineffective against unlearnable

examples, as the experimental outcomes are nearly equivalent to the results of random guessing. In contrast, ST effectively overcomes unlearnable examples. This is because although data poisoning attacks share the same principles as unlearnable examples, they serve different application scenarios. Therefore, defense methods against data poisoning attacks are ineffective for unlearnable examples.

TABLE X

CIFAR-10 TEST ACCURACY (%) OF DIFFERENT DEFENSIVE MEASURES AGAINST DATA POISONING ATTACKS.

Methods	EPI [55]	FrieNDs [56]	ST	ST-CG	ST-Full
EM	9.98	11.76	58.63	80.18	87.05
REM	11.21	10.58	82.11	77.08	78.86
SP	10.54	10.27	42.73	66.75	79.69

V. CONCLUSION

In this paper, we study the mechanism of the data protection method, unlearnable examples that typically cause models to ignore correct semantic features and learn incorrect perturbation features instead. We observed that unlearnable examples mislead models into a trap of unlearnable perturbation learning. We propose the Activation Cluster Measurement (ACM) to quantify the unlearnable perturbation learning degree of a model. Based on that, we propose progressive staged training (ST), a novel stage training framework to gradually slow down the learning process from shallow layers to deep layers and defeat unlearnable examples. Our ST training pipeline breaks all existing state-of-the-art methods and provides a reliable evaluation benchmark for further studies on unlearnable examples.

REFERENCES

[1] K. He, X. Zhang, S. Ren, and J. Sun, "Deep residual learning for image recognition," in *CVPR*. IEEE Computer Society, 2016, pp. 770–778.

- [2] K. Simonyan and A. Zisserman, "Very deep convolutional networks for large-scale image recognition," in *ICLR*, 2015.
- [3] G. Huang, Z. Liu, L. van der Maaten, and K. Q. Weinberger, "Densely connected convolutional networks," in *CVPR*. IEEE Computer Society, 2017, pp. 2261–2269.
- [4] A. Brock, J. Donahue, and K. Simonyan, "Large scale GAN training for high fidelity natural image synthesis," in *ICLR*. OpenReview.net, 2019.
- [5] K. He, G. Gkioxari, P. Dollár, and R. B. Girshick, "Mask R-CNN," in *ICCV*. IEEE Computer Society, 2017, pp. 2980–2988.
- [6] A. Dosovitskiy, L. Beyer, A. Kolesnikov, D. Weissenborn, X. Zhai, T. Unterthiner, M. Dehghani, M. Minderer, G. Heigold, S. Gelly, J. Uszkoreit, and N. Houlsby, "An image is worth 16x16 words: Transformers for image recognition at scale," in *ICLR*. OpenReview.net, 2021.
- [7] Z. Liu, Y. Lin, Y. Cao, H. Hu, Y. Wei, Z. Zhang, S. Lin, and B. Guo, "Swin transformer: Hierarchical vision transformer using shifted windows," in *ICCV*. IEEE, 2021, pp. 9992–10002.
- [8] R. Rombach, A. Blattmann, D. Lorenz, P. Esser, and B. Ommer, "High-resolution image synthesis with latent diffusion models," in *CVPR*. IEEE, 2022, pp. 10674–10685.
- [9] A. Radford, J. W. Kim, C. Hallacy, A. Ramesh, G. Goh, S. Agarwal, G. Sastry, A. Askell, P. Mishkin, J. Clark, G. Krueger, and I. Sutskever, "Learning transferable visual models from natural language supervision," in *ICML*, ser. Proceedings of Machine Learning Research, vol. 139. PMLR, 2021, pp. 8748–8763.
- [10] S. Chen, P. Sun, Y. Song, and P. Luo, "Diffusiondet: Diffusion model for object detection," in *ICCV*. IEEE, 2023, pp. 19773–19786.
- [11] X. Cui, C. Wang, D. Ren, Y. Chen, and P. Zhu, "Semi-supervised image deraining using knowledge distillation," *IEEE Trans. Circuits Syst. Video Technol.*, vol. 32, no. 12, pp. 8327–8341, 2022.
- [12] W. Zhang, Q. Liu, Y. Feng, L. Cai, and P. Zhuang, "Underwater image enhancement via principal component fusion of foreground and background," *IEEE Trans. Circuits Syst. Video Technol.*, vol. 34, no. 11, pp. 10930–10943, 2024.
- [13] W. Liu, W. Li, J. Zhu, M. Cui, X. Xie, and L. Zhang, "Improving nighttime driving-scene segmentation via dual image-adaptive learnable filters," *IEEE Trans. Circuits Syst. Video Technol.*, vol. 33, no. 10, pp. 5855–5867, 2023.
- [14] D. Cheng, L. Chen, C. Lv, L. Guo, and Q. Kou, "Light-guided and cross-fusion u-net for anti-illumination image super-resolution," *IEEE Trans. Circuits Syst. Video Technol.*, vol. 32, no. 12, pp. 8436–8449, 2022.
- [15] B. Jiang, Y. Lu, J. Wang, G. Lu, and D. Zhang, "Deep image denoising with adaptive priors," *IEEE Trans. Circuits Syst. Video Technol.*, vol. 32, no. 8, pp. 5124–5136, 2022.
- [16] A. Krizhevsky and G. Hinton, "Learning multiple layers of features from tiny images," *Handbook of Systemic Autoimmune Diseases*, vol. 1, no. 4, 2009.
- [17] O. Russakovsky, J. Deng, H. Su, J. Krause, S. Satheesh, S. Ma, Z. Huang, A. Karpathy, A. Khosla, M. S. Bernstein, A. C. Berg, and L. Fei-Fei, "Imagenet large scale visual recognition challenge," *Int. J. Comput. Vis.*, vol. 115, no. 3, pp. 211–252, 2015.
- [18] C. Sun, A. Shrivastava, S. Singh, and A. Gupta, "Revisiting unreasonable effectiveness of data in deep learning era," in *ICCV*. IEEE Computer Society, 2017, pp. 843–852.
- [19] D. Mahajan, R. B. Girshick, V. Ramanathan, K. He, M. Paluri, Y. Li, A. Bharambe, and L. van der Maaten, "Exploring the limits of weakly supervised pretraining," in *ECCV (2)*, ser. Lecture Notes in Computer Science, vol. 11206. Springer, 2018, pp. 185–201.
- [20] X. Wang, Y. Peng, L. Lu, Z. Lu, M. Bagheri, and R. M. Summers, "Chestx-ray8: Hospital-scale chest x-ray database and benchmarks on weakly-supervised classification and localization of common thorax diseases," in *CVPR*. IEEE Computer Society, 2017, pp. 3462–3471.
- [21] R. A. Bafghi and D. Gurari, "A new dataset based on images taken by blind people for testing the robustness of image classification models trained for imagenet categories," in *CVPR*. IEEE, 2023, pp. 16261–16270.
- [22] S. Fu, F. He, Y. Liu, L. Shen, and D. Tao, "Robust unlearnable examples: Protecting data privacy against adversarial learning," in *ICLR*. OpenReview.net, 2022.
- [23] D. Yu, H. Zhang, W. Chen, J. Yin, and T. Liu, "Availability attacks create shortcuts," in *KDD*. ACM, 2022, pp. 2367–2376.
- [24] S. Wu, S. Chen, C. Xie, and X. Huang, "One-pixel shortcut: On the learning preference of deep neural networks," in *ICLR*. OpenReview.net, 2023.
- [25] L. Tao, L. Feng, J. Yi, S. Huang, and S. Chen, "Better safe than sorry: Preventing delusive adversaries with adversarial training," in *NeurIPS*, 2021, pp. 16209–16225.
- [26] H. Huang, X. Ma, S. M. Erfani, J. Bailey, and Y. Wang, "Unlearnable examples: Making personal data unexploitable," in *ICLR*. OpenReview.net, 2021.
- [27] J. Ren, H. Xu, Y. Wan, X. Ma, L. Sun, and J. Tang, "Transferable unlearnable examples," in *ICLR*. OpenReview.net, 2023.
- [28] J. Zhang, X. Ma, Q. Yi, J. Sang, Y. Jiang, Y. Wang, and C. Xu, "Unlearnable clusters: Towards label-agnostic unlearnable examples," in *CVPR*. IEEE, 2023, pp. 3984–3993.
- [29] S. Beery, G. V. Horn, and P. Perona, "Recognition in terra incognita," in *ECCV (16)*, ser. Lecture Notes in Computer Science, vol. 11220. Springer, 2018, pp. 472–489.
- [30] R. Geirhos, J. Jacobsen, C. Michaelis, R. S. Zemel, W. Brendel, M. Bethge, and F. A. Wichmann, "Shortcut learning in deep neural networks," *Nat. Mach. Intell.*, vol. 2, no. 11, pp. 665–673, 2020.
- [31] D. Hendrycks, K. Zhao, S. Basart, J. Steinhardt, and D. Song, "Natural adversarial examples," in *Proceedings of the IEEE/CVF Conference on Computer Vision and Pattern Recognition*, 2021, pp. 15262–15271.
- [32] E. Creager, J. Jacobsen, and R. S. Zemel, "Environment inference for invariant learning," in *ICML*, ser. Proceedings of Machine Learning Research, vol. 139. PMLR, 2021, pp. 2189–2200.
- [33] A. Ahmadian and F. Lindsten, "Enhancing representation learning with deep classifiers in presence of shortcut," in *ICASSP*. IEEE, 2023, pp. 1–5.
- [34] L. Fay, E. Cobos, B. Yang, S. Gatidis, and T. Küstner, "Avoiding shortcut-learning by mutual information minimization in deep learning-based image processing," *IEEE Access*, vol. 11, pp. 64070–64086, 2023.
- [35] L. Fowl, M. Goldblum, P. Chiang, J. Geiping, W. Czaja, and T. Goldstein, "Adversarial examples make strong poisons," in *NeurIPS*, 2021, pp. 30339–30351.
- [36] P. S. Segura, V. Singla, J. Geiping, M. Goldblum, T. Goldstein, and D. Jacobs, "Autoregressive perturbations for data poisoning," in *NeurIPS*, 2022.
- [37] S. Farhadkhani, R. Guerraoui, L. N. Hoang, and O. Villemaud, "An equivalence between data poisoning and byzantine gradient attacks," in *ICML*, ser. Proceedings of Machine Learning Research, vol. 162. PMLR, 2022, pp. 6284–6323.
- [38] H. Bansal, F. Yin, N. Singhi, A. Grover, Y. Yang, and K. Chang, "Cleanclip: Mitigating data poisoning attacks in multimodal contrastive learning," in *ICCV*. IEEE, 2023, pp. 112–123.
- [39] T. Qin, X. Gao, J. Zhao, K. Ye, and C.-Z. Xu, "Learning the unlearnable: Adversarial augmentations suppress unlearnable example attacks," in *4th Workshop on Adversarial Robustness In the Real World (AROW), ICCV 2023*, 2023.
- [40] W. Jiang, Y. Diao, H. Wang, J. Sun, M. Wang, and R. Hong, "Unlearnable examples give a false sense of security: Piercing through unexploitable data with learnable examples," in *ACM Multimedia*. ACM, 2023, pp. 8910–8921.
- [41] H. M. Dolatabadi, S. Erfani, and C. Leckie, "The devil's advocate: Shattering the illusion of unexploitable data using diffusion models," in *Proceedings of the IEEE Conference on Secure and Trustworthy Machine Learning (SatML)*, 2024.
- [42] P. S. Segura, V. Singla, J. Geiping, M. Goldblum, and T. Goldstein, "What can we learn from unlearnable datasets?" in *NeurIPS*, 2023.
- [43] N. Srivastava, G. E. Hinton, A. Krizhevsky, I. Sutskever, and R. Salakhutdinov, "Dropout: a simple way to prevent neural networks from overfitting," *J. Mach. Learn. Res.*, vol. 15, no. 1, pp. 1929–1958, 2014.
- [44] A. Krogh and J. A. Hertz, "A simple weight decay can improve generalization," in *NIPS*. Morgan Kaufmann, 1991, pp. 950–957.
- [45] T. DeVries and G. W. Taylor, "Improved regularization of convolutional neural networks with cutout," *arXiv preprint arXiv:1708.04552*, 2017.
- [46] H. Zhang, M. Cissé, Y. N. Dauphin, and D. Lopez-Paz, "mixup: Beyond empirical risk minimization," in *ICLR (Poster)*. OpenReview.net, 2018.
- [47] S. Yun, D. Han, S. Chun, S. J. Oh, Y. Yoo, and J. Choe, "Cutmix: Regularization strategy to train strong classifiers with localizable features," in *ICCV*. IEEE, 2019, pp. 6022–6031.
- [48] E. D. Cubuk, B. Zoph, D. Mané, V. Vasudevan, and Q. V. Le, "Autoaugment: Learning augmentation strategies from data," in *CVPR*. Computer Vision Foundation / IEEE, 2019, pp. 113–123.
- [49] E. D. Cubuk, B. Zoph, J. Shlens, and Q. V. Le, "Randaugment: Practical automated data augmentation with a reduced search space," in *CVPR Workshops*. Computer Vision Foundation / IEEE, 2020, pp. 3008–3017.
- [50] L. Van der Maaten and G. Hinton, "Visualizing data using t-sne." *Journal of machine learning research*, vol. 9, no. 11, 2008.

- [51] I. Sutskever, J. Martens, G. E. Dahl, and G. E. Hinton, “On the importance of initialization and momentum in deep learning,” in *ICML (3)*, ser. JMLR Workshop and Conference Proceedings, vol. 28. JMLR.org, 2013, pp. 1139–1147.
- [52] I. Loshchilov and F. Hutter, “SGDR: stochastic gradient descent with warm restarts,” in *ICLR (Poster)*. OpenReview.net, 2017.
- [53] M. Laskin, K. Lee, A. Stooke, L. Pinto, P. Abbeel, and A. Srinivas, “Reinforcement learning with augmented data,” in *NeurIPS*, 2020.
- [54] S. Zagoruyko and N. Komodakis, “Wide residual networks,” in *BMVC*. BMVA Press, 2016.
- [55] Y. Yang, T. Y. Liu, and B. Mirzasoleiman, “Not all poisons are created equal: Robust training against data poisoning,” in *ICML*, ser. Proceedings of Machine Learning Research, vol. 162. PMLR, 2022, pp. 25 154–25 165.
- [56] T. Y. Liu, Y. Yang, and B. Mirzasoleiman, “Friendly noise against adversarial noise: A powerful defense against data poisoning attack,” in *NeurIPS*, 2022.